RSC Advances

PAPER

View Article Online
View Journal | View Issue

Cite this: *RSC Adv.*, 2018, **8**, 6200

A highly efficient nano-sized Cu_2O/SiO_2 egg-shell catalyst for C–C coupling reactions†

Soohee Kim,[a] Shin Wook Kang,[b] Aram Kim,[a] Mohammad Yusuf,[a] Ji Chan Park *[b] and Kang Hyun Park *[a]

Received 20th December 2017
Accepted 22nd January 2018

DOI: 10.1039/c7ra13490h

rsc.li/rsc-advances

Mesoporous SiO_2-supported Cu_2O nanoparticles as an egg-shell type catalyst were prepared by impregnation method. The obtained Cu_2O/SiO_2 egg-shell nanocatalyst had a large surface area and narrow pore size distribution. In addition, most of the Cu_2O nanoparticles, with sizes around 2.0 nm, were highly dispersed in the mesoporous silica. Accordingly, fast reactant diffusion to the active sites would occur, especially when the active metal sites are selectively located on the outer part of the support, *i.e.*, the outer region of the egg shell. In solvent-free Sonogashira reactions for the synthesis of ynones from acyl chlorides and terminal alkynes, this catalyst exhibited a very high catalytic activity. The excellent catalytic performance can be attributed to the synergistic advantages of mesoporous structure and monodispersed Cu_2O nanoparticles.

Introduction

Supported nanocatalysts exploiting robust metal-oxide structures have been effectively used for various heterogeneous catalytic processes.[1–3] In particular, mesoporous silica supports have been widely used as catalyst support based on their high thermal stability and controllable surfaces as well as their high pore volumes and large surface areas.[4–8] For example, many types of metal/silica nanocatalysts, such as metal@silica yolk–shell[9] and core–shell catalysts,[10,11] have been developed to enhance the catalytic activity and stability against sintering or agglomeration problems of active metal sites.

In recent years, silica-[12,13] and alumina-based[14–16] egg-shell-type catalysts in millimeter scale have been prepared in order to avoid the diffusional restrictions of the reactants for some catalytic reactions, such as Fischer–Tropsch synthesis.[17,18] Simply, fast reactant diffusion to the active sites would occur, especially when the active metal sites are selectively located on the outer part of the support, such as the outer region of the egg shell. However, most egg-shell-type catalysts prepared using the controlled penetration of molten salt have still been focused on the millimeter scale, not the micrometer or nanometer scale.

Accordingly, we utilized the synthesized egg-shell nano-sized particles in the catalytic system. The benefits of the number of potentially reactive small-sized atoms exposed on the surface are expected to include high activity and selectivity.[19] Due to these significant properties, Cu nanoparticles have been used as catalysts for a very broad range of organic transformations, such as click reactions, A^3 coupling, C–H functionalization, borylation, cross-coupling and so on.[20–25]

In this work, we set out to use the Sonogashira protocol, which has emerged as one of the most straightforward and powerful methods for carbon–carbon formation.[26] The products of ynones are a kind of conjugated alkynyl ketones which are useful intermediates of heterocyclic compounds as building blocks for natural products, pharmaceuticals, and molecular organic materials.[27–30] Herein, we report a new type of Cu_2O/SiO_2 egg-shell nanocatalyst as an active and stable catalyst for the synthesis of 1,3-diphenyl-2-propyn-1-one from benzoyl chloride and phenylacetylene.

Experimental

Materials

Copper(II) nitrate trihydrate ($Cu(NO_3)_2 \cdot 3H_2O$, ≥98%), tetraethyl orthosilicate (TEOS, 98%) and hexadecyltrimethylammonium bromide (C_{16}TAB, ≥98%) were purchased from Aldrich. Ammonium hydroxide (NH_4OH, 28% in water) and ethanol (99.9%) were obtained from Junsei and Baker, respectively. The reagents were used as received without further purification.

Synthesis of $mSiO_2$ egg-shell support

NH_4OH aqueous solution (2.5 mL) was added to a mixture of ethanol (100 mL) and distilled water (8.0 mL), and then stirred for 5 min. TEOS (10 mL) was added to the prepared solution and stirred for 2 h at room temperature. The resulting silica particles were precipitated by centrifugation at 8000 rpm for 20 min, then washed thoroughly with ethanol (100 mL). The dispersed

[a]*Department of Chemistry, Chemistry Institute for Functional Materials, Pusan National University, Busan, 46241, Republic of Korea. E-mail: chemistry@pusan.ac.kr*
[b]*Clean Fuel Laboratory, Korea Institute of Energy Research, Daejeon, 34129, Korea. E-mail: jcpark@kier.re.kr*

† Electronic supplementary information (ESI) available. See DOI: 10.1039/c7ra13490h

silica in ethanol (100 mL) was diluted with distilled water (200 mL). A solution of C_{16}TAB (1.2 g, 3.3 mmol) dissolved in a solvent mixture of distilled water (20 mL) and ethanol (10 mL) was injected into the diluted silica solution. This mixture was vigorously stirred under ambient conditions for 30 min. After 30 min, TEOS (2.15 mL, 9.6 mmol) was added to the reaction solution and stirred for 12 h. The resulting $mSiO_2$ egg-shell nanoparticles were precipitated by centrifugation at 8000 rpm for 10 min, and then washed thoroughly with ethanol (150 mL) and acetone (150 mL). After drying at 100 °C in a drying oven, the white powder was placed in an alumina boat in a tube-type furnace, heated at a ramp rate of 4 °C min^{-1} to 500 °C, and calcined at 500 °C for 8 h in air.

Synthesis of nano-sized Cu_2O/SiO_2 egg-shell catalyst

For synthesis of the Cu_2O/SiO_2 egg-shell nanocatalyst containing 10 wt% Cu, aqueous copper nitrate solution (8.74 M, 0.1 mL) was added dropwise onto the $mSiO_2$ egg-shell support (0.5 g). Infiltration was performed by grinding the mixture under ambient conditions for 10 min until the powder was homogeneously pale blue. Next, the mixed powder was placed in an autoclave reactor and aged in an oven at 120 °C. After aging for 24 h, the sample was cooled in ambient atmosphere and transferred into an alumina boat in a tube-type furnace. Finally, the copper-incorporated silica powder with pale blue color was slowly heated under H_2 flow of 200 mL min^{-1}, at a ramp rate of 2.7 °C min^{-1}, to 350 °C. The sample was thermally treated under continuous H_2 flow at 350 °C for 4 h. After calcination, the resulting powder with pale green color was cooled down to room temperature.

Characterization

High-resolution transmission electron microscopy (HRTEM) was performed using a Tecnai TF30 ST and a Titan double Cs-corrected TEM instrument (Titan cubed G2 60-300). Energy-dispersive X-ray spectroscopy (EDS) elemental mapping data were collected using a higher-efficiency detection system (Super-X detector). High-power X-ray powder diffraction (XRD) (Rigaku D/MAX-2500, 18 kW) was also used for the analysis. N_2 sorption isotherms were measured at 77 K with a Tristar II 3020 surface area analyser. Before the measurement, the sample was degassed under N_2 flow at 300 °C for 4 h.

Activity tests

In a typical run of the solvent-free Sonogashira coupling reaction,[31] 0.50 mmol phenylacetylene, 0.75 mmol benzoyl chloride, 4.0 equiv. triethylamine (base) and 1.0 mol% Cu_2O/SiO_2 egg-shell nanocatalyst were mixed in a 25 mL oven-dried Schlenk reaction tube. After reacting in argon atmosphere at 80 °C for 12.0 h, the reaction mixture was filtered and extracted with dichloromethane, then analyzed using a gas chromatograph (SHIMADZU, GCMS-QP2010 SE).

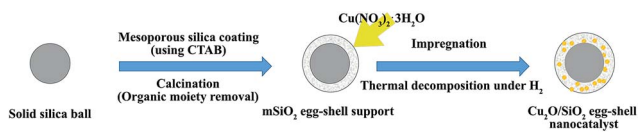

Fig. 1 Schematic illustration of the synthesis of the Cu_2O/SiO_2 egg-shell nanocatalyst.

Results and discussion

Preparation of Cu_2O/SiO_2 egg-shell nanocatalyst

Fig. 1 shows a brief synthetic scheme for the Cu_2O/SiO_2 egg-shell nanocatalyst. The solid SiO_2 cores within mesoporous SiO_2 shells ($mSiO_2$ egg-shell supports) were prepared by a modified sol–gel method as reported in the literature.[32] The transmission electron microscopy (TEM) images show uniform silica nanospheres with average diameter of 305 ± 18 nm (Fig. 2a and b). Mesoporous silica shells were coated onto the silica nanospheres using the cationic surfactant C_{16}TAB, both as a structure-directing agent and a sacrificial porogen. The TEM images show $mSiO_2$ egg-shell supports around 435 nm, larger than the initial SiO_2 nanospheres (Fig. 2c). The thickness of the uniformly coated mesoporous silica shell on the solid silica core was observed as approximately 65 nm in the HRTEM image (Fig. 2d). Ordered mesoporous channels in the silica shell could be generated by thermal removal of C_{16}TAB.

Next, the copper(I) oxide/silica catalyst (designated as Cu_2O/SiO_2 egg-shell nanocatalyst), with controlled Cu content of 10 wt% on the basis of Cu converted from the copper nitrate salt after thermal treatment, was prepared by incorporating Cu_2O particles formed inside the pores of $mSiO_2$ egg-shell supports. Impregnation of copper nitrate and subsequent hydrogen reduction yielded small and uniform Cu_2O particles in channel-like SiO_2 pores. The chemical reaction for the thermal decomposition of $Cu(NO_3)_2$ and Cu_2O formation is proposed to be:

$$2Cu(NO_3)_2\,(s) + H_2\,(g) \rightarrow Cu_2O\,(s) + 4NO_2\,(g) + H_2O\,(g) + O_2\,(g)$$

The TEM image indicates that the Cu_2O nanoparticles were incorporated well into the mesopores of silica (Fig. 3a). The

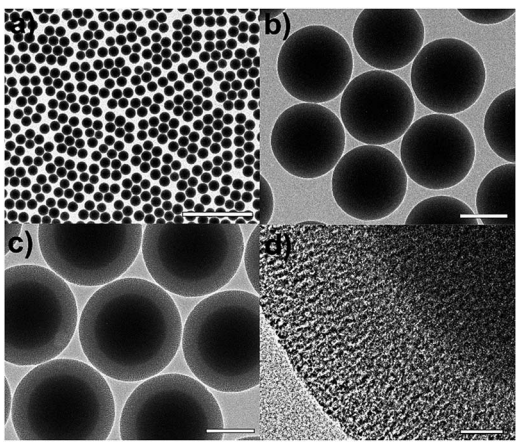

Fig. 2 (a and b) TEM images of silica nanospheres, and (c) TEM and (d) HRTEM images of $mSiO_2$ egg-shell support. The bars represent 2 μm (a), 200 nm (b, c), and 20 nm (d).

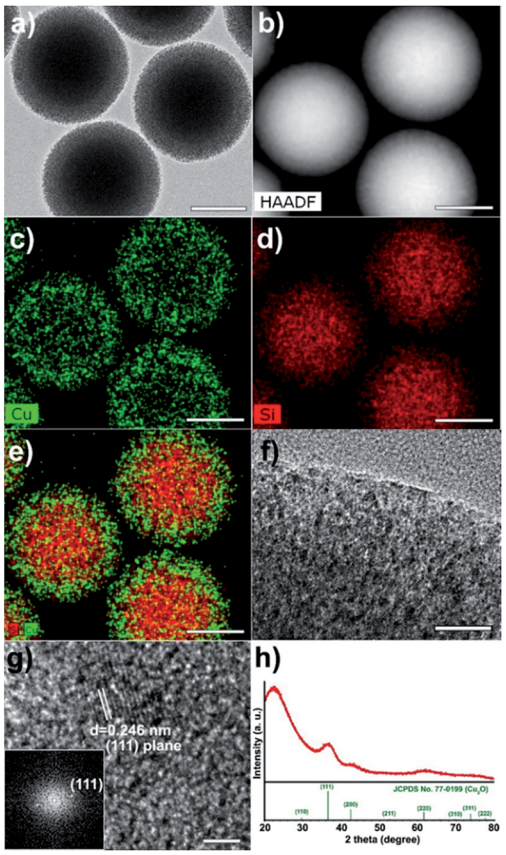

Fig. 3 (a) TEM and (b) HADDF images, (c–e) scanning TEM image with elemental mapping, and (f and g) HRTEM images with the corresponding FT pattern (inset of g), and (h) XRD spectrum of Cu_2O/SiO_2 egg-shell nanocatalyst. The bars represent 200 nm (a–e), 20 nm (f), and 2 nm (g).

high-angle annular dark-field scanning transmission electron microscopy (HAADF-STEM) image also shows regions of varying brightness. Relatively bright spots correspond to Cu_2O nanoparticles (Fig. 3b). In the elemental mapping, Cu (green) and Si (red) are confirmed (Fig. 3c–e). The magnified TEM image shows black dots in channel-like pores, indicating small Cu_2O crystals (Fig. 3f). The HRTEM image and the corresponding Fourier-transform (FT) pattern indicate the single crystalline nature of the Cu_2O particle (Fig. 3g). The inside particle size was observed to be between 2 and 3 nm. The lattice distance of 0.246 nm between neighbouring fringes corresponds to the (111) lattice spacing in cubic phase Cu_2O. In the XRD pattern, Cu_2O/SiO_2 egg-shell nanocatalyst is also well matched with cuprite (Fig. 3h, space group: *Pn3m*, JCPDS no. 77-0199). The broad peak at $2\theta = 36.5^\circ$ corresponds to the (111) plane of Cu_2O. The mean particle size was estimated to be 2.0 nm using the Debye–Scherrer equation from the full width at half maximum (fwhm) of the (111) peak.

N_2 sorption experiments for the pristine $mSiO_2$ egg-shell support and the Cu_2O/SiO_2 egg-shell nanocatalyst show type IV adsorption–desorption hysteresis (Fig. 4a). The Brunauer–Emmett–Teller (BET) surface areas were calculated to be 481.2 $m^2\ g^{-1}$ for the pristine $mSiO_2$ egg-shell support and

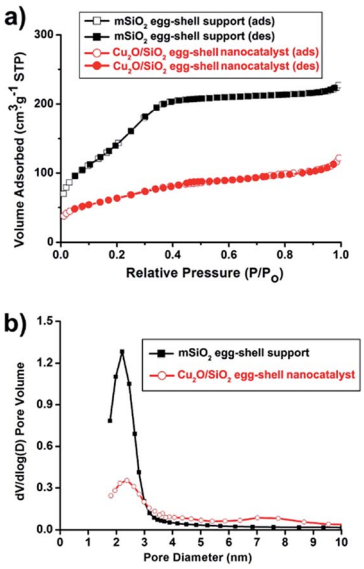

Fig. 4 (a) N_2 adsorption/desorption isotherms and (b) pore size distribution diagrams using the Barrett–Joyner–Halenda (BJH) method from the adsorption branches of the $mSiO_2$ egg-shell support and the Cu_2O/SiO_2 egg-shell nanocatalyst.

228.9 $m^2\ g^{-1}$ for the Cu_2O/SiO_2 egg-shell nanocatalyst, respectively. The total pore volume of the Cu_2O/SiO_2 egg-shell nanocatalyst was found to be 0.19 $cm^3\ g^{-1}$, which is about 54% of the pristine $mSiO_2$ egg-shell support (0.35 $cm^3\ g^{-1}$). The significant decrease in pore volume of the Cu_2O/SiO_2 egg-shell nanocatalyst was attributed to the occupied copper oxide nanoparticle in the silica pore. The pore size distributions of the initial $mSiO_2$ egg-shell support and Cu_2O/SiO_2 egg-shell nanocatalyst were identically observed in the range of 2–3 nm, well reflecting the embedded Cu_2O crystallite size (Fig. 4b).

Sonogashira coupling reactions

We explored the catalytic performance of the synthesized Cu_2O/SiO_2 egg-shell nanocatalyst toward Sonogashira coupling reactions. It was found that supported copper nanoparticles efficiently catalyzed the synthesis of ynones of acyl chlorides and alkynes.[33,34] In this type of reaction, Cu_2O nanoparticles activate phenylacetylene to form copper(I) acetylide compounds, which subsequently react with acyl chloride.[35,36] In addition, this reaction does not require any ligand and palladium source under solvent-free conditions.

The effect of several factors, such as reaction time, temperature, base, and amount of catalyst, was studied. The results are listed in Table 1. Initially, it was demonstrated that changes in the catalyst loading have marked impacts on the conversions. It was shown that increasing the amount of catalyst loading from 1 mol% to 1.5 mol% resulted in higher conversion (86%) (Table 1, entries 1 and 2). In order to improve the conversion of the reaction, we increased the temperature to 80 °C, which resulted in higher conversion than at 40 °C (Table 1, entries 3 and 4). Thereafter, when the reaction time was extended to 12 h, the conversion of 99% was achieved (Table 1, entry 5). In addition,

Table 1 Solvent-free Sonogashira reactions for the synthesis of ynones from acyl chlorides and terminal alkynes catalyzed by Cu_2O/SiO_2 egg-shell nanocatalyst[a]

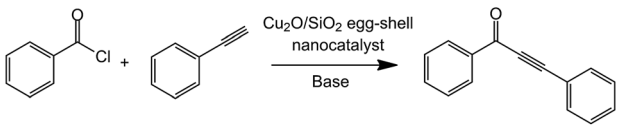

Entry	Cat. (mol%)	Temp (°C)	Base (eq.)	Time (h)	Conv. (%)	Select. (%)
1	1	40	3	8	66	99
2	1.5	40	3	8	86	98
3	1	80	3	8	93	97
4	1.5	80	3	8	100	98
5	1	80	3	12	99	97
6	—	80	4	12	8	0
7	1	80	—	12	5	0
8	1	80	4	12	100	99
9	Recover from #8	80	4	12	100	99
10	Recover from #9	80	4	12	98	99
11	Recover from #10	80	4	12	94	99
12[b]	1	80	4	12	76	99
13[c]	1	80	4	12	100	91
14	Recover from 13	80	4	12	7	0

[a] Reaction conditions: phenylacetylene (0.50 mmol), benzoyl chloride (0.75 mmol), base Et_3N, cat. Cu_2O/SiO_2 egg-shell nanocatalyst, Ar atmosphere. Determined by using gas chromatography-mass spectrometery (GC-MS). [b] Cat. commercial Cu_2O powder purchased from Aldrich (no. 208825). [c] Cat. conventional SiO_2-supported Cu_2O catalyst.

when the amount of base was increased (4.0 equiv.), the conversion was 100% (Table 1, entry 8), and the selectivity was 99% owing to Cu_2O/SiO_2 egg-shell nanocatalyst hindering the homocoupling of benzoyl chloride and phenylacetylene. Subsequently, the optimized reaction conditions were phenylacetylene (0.5 mmol), benzoyl chloride (0.75 mmol), Cu_2O/SiO_2 egg-shell nanocatalyst (1 mol%), and Et_3N (4 equiv.) at 80 °C for 12 h under Ar atmosphere. Furthermore, when we conducted the reaction without base or catalysts under the optimized reaction conditions, each reaction hardly proceeded

Table 2 Substrate study for the coupling reaction of alkynes and acyl chlorides[a]

Entry	Acyl chloride	Alkyne	Product	Conv. (%)	Select. (%)
1		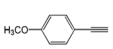	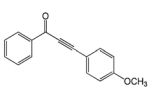	66	100
2			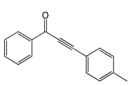	98	99
3		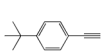	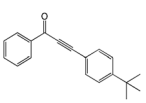	88	87
4		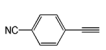	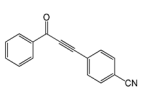	89	98
5		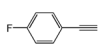	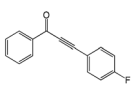	98	85
6			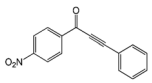	100	100

[a] Reaction conditions: alkyne (0.5 mmol), acyl chloride (0.75 mmol), Et_3N (4.0 equiv.), 1.0 mol% Cu_2O/SiO_2 egg-shell nanocatalyst, 80 °C, 12.0 h.

(Table 1, entries 6 and 7). Thus, a basic medium is essential for these cross-coupling reactions. However, under the same condition, but replacing the Cu_2O/SiO_2 egg-shell nanocatalyst with commercial Cu_2O powder as catalyst, the coupling reaction was obtained with lower conversion and selectivity (Table 1, entry 12). Even though the conventional SiO_2-supported Cu_2O catalyst showed similar catalytic activity, low reusability was obtained due to decomposed catalyst structures (Table 1, entries 13 and 14). The Cu_2O/SiO_2 egg-shell nanocatalyst was recycled up to three times without any loss of its initial high activity (>94%) in subsequent experiments (Table 1, entries 9–11). Therefore, this indicates that the high dispersion and excellent accessibility of the Cu_2O NPs cause the high efficiency of the Cu_2O/SiO_2 egg-shell nanocatalysts. Moreover, they showed enhanced catalytic activity and facilitated considerably positive synergistic effects with nanosized porous support substrates,[37–40] as compared to Cu_2O nanoparticles without the mesoporous support.[41] All reactions are carried out in the void inside the shell. In other words, the egg-shell structure acts as a "nanoreactor framework", which contains enough space between the core and shell. Each of the active nanoparticles experiences a homogeneous environment in a void surrounded by the silica shell. We also studied the role of solvent system under the optimized conditions (ESI, Table S1†).[42] In addition, when we carried out the reactions with dipolar aprotic solvents such as dimethylformamide (DMF) and tetrahydrofuran (THF), results were inferior because of the formation of the corresponding anhydride as a by-product. However, the reaction under nonpolar solvent, such as toluene, gave 84% conversion. Therefore, all reactions were performed neat under anhydrous conditions. Encouraged by the above results, with these optimized reaction conditions, the scope of the developed protocol was extended for the synthesis of ynone derivatives using different substrates (Table 2). As shown in Table 2, most of the substrates gave good conversions despite electron-donating substituents (methyl, *tert*-butyl and methoxy groups) and electron-withdrawing substituents (fluoro, cyano groups). Furthermore, benzoyl chloride substituted with a nitro group still gave the corresponding ynones with good conversion rate (Table 2, entry 6).

Conclusions

In this paper, egg-shell-type mesoporous silica-supported copper nanoparticle catalyst was prepared. The obtained Cu_2O/SiO_2 egg-shell nanocatalyst had a large surface area and narrow pore size distribution. In addition, most of the Cu_2O nanoparticles, with sizes around 2.0 nm, were highly dispersed in the mesoporous silica. Accordingly, fast reactant diffusion to the active sites would occur, especially when the active metal sites are selectively located on the outer part of the support, *i.e.*, the outer region of the egg shell. As a result, they enhanced the reaction kinetics. In palladium-free, ligand-free and solvent-free Sonogashira reactions for the synthesis of ynones from acyl chlorides and terminal alkynes, this catalyst exhibited a very high catalytic activity. The excellent catalytic performance can be attributed to the synergistic advantages of the mesoporous structure and the monodispersed Cu_2O nanoparticles. The egg-shell structure acts as a "nanoreactor framework", which contains sufficient space and catalytically active surface within its structure. The egg-shell nanoparticles have potential for application as nanoreactors and catalysts, drug delivery carriers, and surface-enhanced Raman scattering substrates.

Conflicts of interest

There are no conflicts to declare.

Acknowledgements

This research was supported by Basic Science Research Program through the National Research Foundation of Korea (NRF) and the Research and Development Program of the Korea Institute of Energy Research (KIER) (No. B8-2461-01), and funded by the Ministry of Science, ICT & Future Planning (NRF-2017R1A4A1015533 and NRF-2017R1D1A1B03036303).

References

1 M. J. Albaladejo, F. Alonso, Y. Moglie and M. Yus, *Eur. J. Org. Chem.*, 2012, **2012**(16), 3093–3104.
2 T. D. Nguyen, C. T. Dinh, D. Mrabet, M. N. Tran-Thi and T. O. Do, *J. Colloid Interface Sci.*, 2013, **394**, 100–107.
3 M. L. Kantam, V. S. Jaya, B. Sreedhar, M. M. Rao and B. M. Choudary, *J. Mol. Catal. A: Chem.*, 2006, **256**(1–2), 273–277.
4 Z. Tai, M. A. Isaacs, C. M. Parlett, A. F. Lee and K. Wilson, *Catal. Commun.*, 2017, **92**, 56–60.
5 M. V. Zakharova, F. Kleitz and F.-G. Fontaine, *Dalton Trans.*, 2017, **46**(12), 3864–3876.
6 J. Ren, P. Hao, W. Sun, R. Shi and S. Liu, *Chem. Eng. J.*, 2017, **328**, 673–682.
7 Q. Gao, H. T. Li, Y. Ling, B. Han, K. S. Xia and C. G Zhou, *Microporous Mesoporous Mater.*, 2017, **241**, 409–417.
8 P. Verma, K. Yuan, Y. Kuwahara, K. Mori and H. Yamashita, *Appl. Catal., B*, 2018, **223**, 10–15.
9 J. Fang, Y. Zhang, Y. Zhou, S. Zhao, C. Zhang, H. Zhang, X. Sheng and K. Wang, *Langmuir*, 2017, **33**(11), 2698–2708.
10 Y. Han, B. Wen and M. Zhu, *Catalysts*, 2017, **7**(1), 21–31.
11 X. Zhang, Y. Zhang, X. Zhang, S. Li and Y. Huang, *J. Hazard. Mater.*, 2017, **337**, 1–9.
12 S. A. Gardezi, J. T. Wolan and B. Joseph, *Appl. Catal., A*, 2012, **447**, 151–163.
13 Y. Zhuang, M. Claeys and E. Van Steen, *Appl. Catal., A*, 2006, **301**(1), 138–142.
14 J. Kolena, G. Šťávová, P. Morávek and K. Štěpánek, *Univers. J. Chem.*, 2017, **5**(1), 19–28.
15 E. H. Cho, K. Y. Koo, H. W. Lee, Y.-K. Park, W. L. Yoon and C. H. Ko, *Int. J. Hydrogen Energy*, 2017, **42**, 18350–18357.
16 M.-S. Jang, E. H. Cho, K. Y. Koo, W. L. Yoon and C. H. Ko, *Appl. Catal., A*, 2017, **530**, 211–216.
17 S. A. Gardezi, L. Landrigan, B. Joseph and J. T. Wolan, *Ind. Eng. Chem. Res.*, 2011, **51**(4), 1703–1712.

18 E. Peluso, C. Galarraga and H. De Lasa, *Chem. Eng. Sci.*, 2001, **56**(4), 1239–1245.
19 K. Larmier, S. Tada, A. Comas-Vives and C. Copéret, *J. Phys. Chem. Lett.*, 2016, **7**(16), 3259–3263.
20 M. B. Gawande, A. Goswami, F.-X. Felpin, T. Asefa, X. Huang, R. Silva, X. Zou, R. Zboril and R. S. Varma, *Chem. Rev.*, 2016, **116**(6), 3722–3811.
21 M. R. Decan, S. Impellizzeri, M. L. Marin and J. C. Scaiano, *Nat. Commun.*, 2014, **5**, 4612.
22 H. Cheng, J. Wen and C. Bolm, *Chem.–Eur. J.*, 2017, **23**, 12100–12103.
23 M. Sengoden, A. Bhowmick and T. Punniyamurthy, *Org. Lett.*, 2016, **19**(1), 158–161.
24 L. Mao, K. l. n. J. Szabó and T. B. Marder, *Org. Lett.*, 2017, **19**(5), 1204–1207.
25 S. Thapa, P. Basnet and R. Giri, *J. Am. Chem. Soc.*, 2017, **139**(16), 5700–5703.
26 R. Chinchilla and C. Nájera, *Chem. Rev.*, 2007, **107**(3), 874–922.
27 D. B. Grotjahn, S. Van, D. Combs, D. A. Lev, C. Schneider, M. Rideout, C. Meyer, G. Hernandez and L. Mejorado, *J. Org. Chem.*, 2002, **67**(26), 9200–9209.
28 J. P. Waldo and R. C. Larock, *J. Org. Chem.*, 2007, **72**(25), 9643–9647.
29 Z. Wang, L. Li and Y. Huang, *J. Am. Chem. Soc.*, 2014, **136**(35), 12233–12236.
30 B. M. Trost and A. Quintard, *Org. Lett.*, 2012, **14**(17), 4698–4700.
31 M. Bakherad, A. Keivanloo and S. Samangooei, *Tetrahedron Lett.*, 2012, **53**(43), 5773–5776.
32 P.-W. Xiao, L. Zhao, Z.-Y. Sui and B.-H. Han, *Langmuir*, 2017, **33**(24), 6038–6045.
33 K. Wang, L. Yang, W. Zhao, L. Cao, Z. Sun and F. Zhang, *Green Chem.*, 2017, **19**, 1949–1957.
34 W. Sun, Y. Wang, X. Wu and X. Yao, *Green Chem.*, 2013, **15**(9), 2356–2360.
35 H. Lang, A. Jakob and B. Milde, *Organometallics*, 2012, **31**, 7661–7693.
36 J. Santandrea, A.-C. Bédard and S. K. Collins, *Org. Lett.*, 2014, **16**, 3892–3895.
37 Z. Zhang, J. C. Jung and N. Yan, *Nanoscale*, 2016, **8**, 19684–19695.
38 X. Yan, J. Yang, L. Ma, X. Tong, Y. Wang, G. Jin and X.-Y. J. Guo, *J. Solid State Electrochem.*, 2015, **19**, 3195–3199.
39 J. Zhang, Y. Wang, C. Yu, X. Shu, L. Jiang, J. Cui, Z. Chen, T. Xiee and Y. Wu, *New J. Chem.*, 2014, **38**, 4975–4984.
40 W. Yin, R. Liu, G. He, W. Lv and H. Zhu, *RSC Adv.*, 2014, **4**, 37773–37778.
41 M. A. Bhosale, T. Sasakib and B. M. Bhanage, *Catal. Sci. Technol.*, 2014, **4**, 4274–4280.
42 H. Yuan, Y. Shen, S. Yu, L. Shan, Q. Sun and W. Zhang, *Synth. Commun.*, 2013, **43**, 2817–2823.